Misfit Nanotubes

DOI: 10.1002/ange.201404189

Lanthanide-Based Functional Misfit-Layered Nanotubes**

*Leela S. Panchakarla, Ronit Popovitz-Biro, Lothar Houben, Rafal E. Dunin-Borkowski, and Reshef Tenne**

Abstract: *The synthesis of nanotubes from layered compounds has generated substantial scientific interest. "Misfit" layered compounds (MLCs) of the general formula $[(MX)_{1+x}]_m[TX_2]_n$, where M can include Pb, Sb, rare earths; T = Cr, Nb, and X = S, Se can form layered structures, even though each sub-system alone is not necessarily a layered or a stable compound. A simple chemical method is used to synthesize these complex nanotubes from lanthanide-based misfit compounds. Quaternary nanotubular structures formed by partial substitution of the lanthanide atom in nanotubes by other elements are also confirmed. The driving force and mechanism of formation of these nanotubes is investigated by systematic temperature and time-dependent studies. A stress-inducement mechanism is proposed to explain the formation of the nanotubes. The resulting materials may find applications in fields that include thermoelectrics, light emitters, and catalysis and address fundamental physical issues in low dimensions.*

The synthesis of carbon nanotubes[1] and subsequently inorganic nanotubes (INTs) from layered compounds[2] has generated substantial scientific interest. The driving force for the formation of such seamless nanostructures stems from the healing of dangling bonds on the rim of the layers.[3] In this way, nanotubes have been prepared from a variety of layered materials, including WS_2, MoS_2, BN, and SnS_2.[2d,4] "Misfit" layered compounds (MLCs) of the general formula $[(MX)_{1+x}]_m[TX_2]_n$, where M = Pb, Sb, rare earths; T = Cr, Nb, and X = S, Se[5] can form layered structures, even though each sub-system alone is not necessarily a layered or a stable compound. MLCs demonstrate superior thermoelectric behavior,[6] superconductivity,[7] and a host of other interesting magnetic, optical, and electrical properties. The in-plane (*a*-*b*) periodicities of the different layers in the misfit structure are mutually incommensurate along at least one direction,[5a–c] often leading to folding of the layers and scrolling.[8] A combination of these two independent stimuli, that is, the incommensurability of the misfit lattice and the reactivity of the rim atoms, provides a new strategy to synthesize misfit nanotubes, such as SnS-SnS_2 and PbS-NbS_2, which have recently been reported.[9]

In contrast to misfit compounds such as PbS-NbS_2, which are made of two stable subunits, $(LaS)_{1.2}CrS_2$ (sometimes named $LaCrS_3$ or LaS-CrS_2) is a misfit compound with triclinic structure ($a = 17.2$; $b = 5.94$; $c = 66.2$ Å; $\alpha = 95.3°$; $\beta = 90.3°$)[10] comprising triclinic double layers of LaS (space group: $C\bar{1}$)[5a] and pseudo hexagonal layers (denoted by a pseudo orthohexagonal reciprocal-lattice mesh) of CrS_2 (space group: $C\bar{1}$),[5a] which are stacked together alternately, with the latter phase being metastable and not known in pristine form in the bulk phase. However, metastable CrS_2 forms a stable hexagonal layered structure upon intercalating alkali, Cu, or Ag atoms,[11] with six S atoms coordinated octahedrally to the Cr atom.[11] Whereas in misfit compounds, such as PbS-NbS_2, van der Waals forces play the largest role in "gluing" the layers together, here the stability of the $LaCrS_3$ misfit layered structure is gained mostly through charge transfer from the LaS slab to the CrS_2 (VS_2).[12]

Herein, we demonstrate a simple chemical method to synthesize nanotubes from a new family of misfit compounds of the type LnS-TS_2, where Ln are rare-earth-metal atoms and T are transition-metal atoms, such as Cr and V. Partial substitution of the Ln atom in nanotubes by other elements has also been confirmed. The growth mechanism of these nanotubes differs substantially from that of the previously reported misfit nanotubes.[9] Various many-body effects, including topological insulator behavior[13] and phase slip,[14] have recently been observed by measuring the transport properties of nanowires. In contrast to nanowires, nanotubes are free of surface defects and consequently are expected to reveal truly unique many-body physical phenomena in one dimension.

Either $LaCrO_3$ or a mixture of $La(OH)_3$ and $Cr(OH)_3$, prepared by reacting the respective nitrates with ammonium hydroxide, was annealed at high temperature (825–900 °C) in the presence of H_2/H_2S gases, resulting in the formation of large quantities of LaS-CrS_2 nanotubes/nanoscrolls. Figure 1 shows SEM images of the as-synthesized LaS-CrS_2 nanotubes, which grow vertically from the substrate. Open-ended nanotubes, nanoscrolls, and semi-folded sheets of LaS-CrS_2 are

[*] Dr. L. S. Panchakarla, Prof. R. Tenne
Department of Materials and Interfaces
Weizmann Institute of Science, Rehovot, 76100 (Israel)
E-mail: Reshef.Tenne@weizmann.ac.il
Homepage: http://www.weizmann.ac.il/materials/tenne/
Dr. R. Popovitz-Biro
Chemical Research Support Department
Weizmann Institute of Science, Rehovot, 76100 (Israel)
Dr. L. Houben, Prof. R. E. Dunin-Borkowski
Ernst Ruska-Centre for Microscopy and Spectroscopy with Electrons and Peter Grünberg Institute, Forschungszentrum Jülich GmbH, 52425 Jülich (Germany)

[**] This research was supported by the ERC grant INTIF 226639, the EU ITN 317451 grant, and a grant from the Israel Science Foundation. R.T. acknowledges the support of the Harold Perlman Foundation, the Irving and Azelle Waltcher Foundation in honor of Prof. M. Levy, and the Irving and Cherna Moskowitz Center for Nano and Bio-Nano Imaging. He holds the Drake Family chair in Nanotechnology and is the Director of the Helen and Martin Kimmel Center for Nanoscale Science. L.S.P. would like to thank the PBC Program of the Government of Israel for a post-doctoral fellowship.

Supporting information for this article is available on the WWW under http://dx.doi.org/10.1002/anie.201404189.

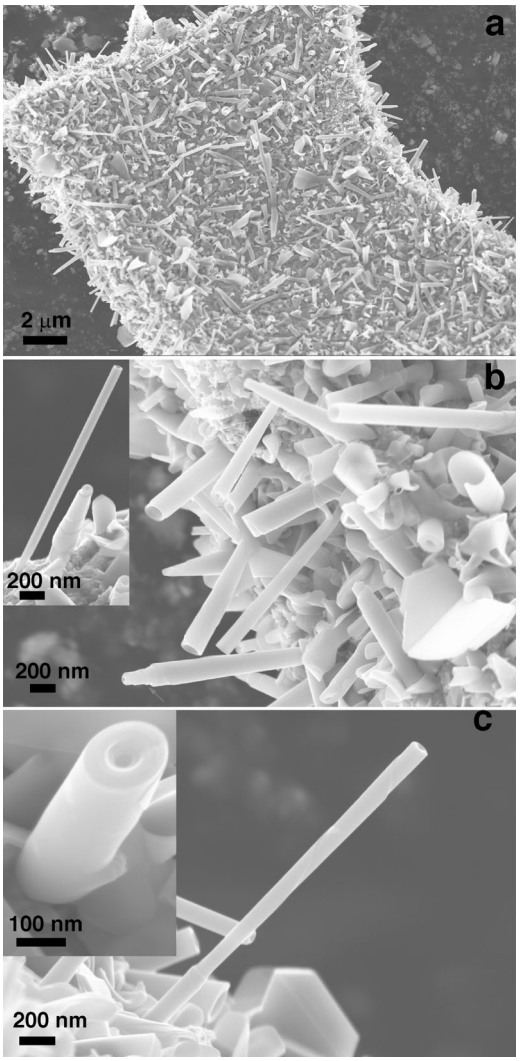

Figure 1. a) low- and b), c) high-magnification SEM images of LaS-CrS_2 nanoscrolls and nanotubes. The insets in (b) and (c) show single nanotube and single nanoscroll images, respectively. Steps on one of the nanoscrolls are marked with an arrow in (b).

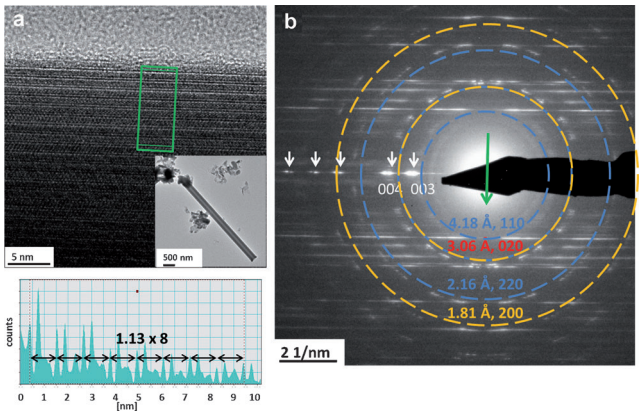

Figure 2. a) HRTEM image of a LaS-CrS_2 nanotube, shown alongside a line profile (bottom) obtained from the region indicated by the green rectangle. A low-magnification TEM image of the same tube is shown as an inset. b) SAED pattern taken from the area shown in (a). The tube axis and basal reflections are marked with green and white arrows, respectively. Spots corresponding to the same interplanar spacings are marked by segmented circles and measured values, with corresponding Miller indices indicated. Blue and orange colors indicate LaS and CrS_2 sub-systems, respectively. The label in red indicates spots originating from both sub-systems.

observed. The diameters of the tubes range from 50 to 300 nm, while their lengths range between 0.5 and 3 μm.

LaS-CrS_2 nanotubes were characterized by transmission electron microscopy (TEM) and high-resolution TEM (HRTEM). Figure 2a shows a typical HRTEM image of a LaS-CrS_2 nanotube synthesized at 900 °C. The superstructure of alternating LaS and CrS_2 layers has a periodicity of 1.13 nm (see the line profile at the bottom of Figure 2a). Selected-area electron diffraction (SAED) also confirmed the superstructure periodicity (Figure 2b). The interplanar spacings reported here are similar (ca. 6% higher) when compared with values for bulk $(LaS)_{1.2}CrS_2$ (see Table 1). There are 12 pairs of {110} and {220} reflections of LaS on a circle, equally azimuthally distributed with *d*-spacings of 4.18 and 2.16 Å, respectively. The multiplicity factor of these planes is four, indicating that there are three LaS sheets with different rolling vectors present in the same tube. Twelve sets of spots are aplit by similar angles (12°); such a splitting arises from chiral folding of the layers with a chiral angle of 6°, which is equal to half of the azimuthal splitting of the spots, (12° in this case). There are 12 sets of {200} and {020} reflections of CrS_2 equally distributed azimuthally on the circle with *d*-spacings of 1.81 and 3.06 Å, respectively. Couple of both the (200) and the (020) reflections match with the tubule axis, indicating that two different rolling vectors of CrS_2 layers are present in the same tube. The chiral angles of the layers are 6° in this case. The *b*-directions of LaS and CrS_2 are parallel, and the lattice parameters are commensurate in this direction. Thus, 12 sets of observed {020} planes with a *d*-spacing of 3.06 Å originate from both the LaS and the CrS_2 layers. An HRTEM image and an SAED pattern of one of the LaS-CrS_2 nanoscrolls are shown in the Supporting Information, Figure S1.

The one-to-one stacking order of the LnS-TS_2 superstructure (or in short O-T, where O and T stand for LnS, TS_2 subunits, respectively) in the nanotube is necessary for securing the stability of the hexagonal layered structure of the CrS_2 (VS_2) by charge transfer from the LnS layer, which has an extra electron with a high chemical potential.[5a] The following observations were also made after analysis of several LaS-CrS_2 tubular structures: 1) missing (005) reflections in SAED patterns; 2) common chiral angles for the LaS and CrS_2 subunits; 3) orientation angles between different LaS layers within the same tube/scroll of 60° with respect to one another. The structure factor of the (005) and (008) reflections in a perfectly ordered LnS-CrS_2 superstructure is two orders of magnitude smaller than that for the (003) reflections (see the Supporting Information for a calculation of the structure factors of {00*l*} planes). The presence of only an O-T superstructure along with the missing (005) reflections therefore indicates strong interaction between the LnS and CrS_2 layers. This strong interaction results from charge

Table 1: Summary of data for the synthesized nanotubes in this work with their lattice parameters obtained from electron diffraction.[a]

Precursor	Compound	Yield	$2a_2/a_1$		Lattice parameters [Å]		
					a	*b*	*c*
mixture of hydroxides, or $LaCrO_3$ powder	LaS-CrS_2	5	1.14	LaS	6.02 (5.752)	6.02 (5.936)	11.3 (11.04)
				CrS_2	3.44 (3.435)	6.02 (5.936)	11.3 (11.05)
mixture of hydroxides	CeS-CrS_2	5	1.14	CeS	6.0	6.0	11.2
				CrS_2	3.44	6.0	11.2
mixture of hydroxides	GdS-CrS_2	3	1.27	GdS	5.82 (5.454)	6.26 (5.810)	11.0 (21.46)
				CrS_2	3.7 (3.451)	6.26 (5.802)	11.0 (21.46)
mixture of hydroxides	TbS-CrS_2	3	1.18	TbS	5.66	5.28	10.5
				CrS_2	3.34	5.28	10.5
mixture of hydroxides	YS-CrS_2	2	1.27	YS	5.34 (5.41)	5.82 (5.78)	10.7 (10.7)
				CrS_2	3.39 (3.46)	5.82 (5.78)	10.7 (10.7)
Mixture of $La(OH)_3$ + $VOSO_4$	LaS-VS_2	1	1.14	LaS	6.02 (5.705)	6.02 (5.828)	11.4 (22.21)
				VS_2	3.44 (3.366)	6.02 (5.828)	11.4 (22.21)
mixture of hydroxides	$LaS(SrS)_{0.2}$-CrS_2	5	1.28	$LaS(SrS)_{0.2}$	5.82	5.82	11.1
				CrS_2	3.44	5.82	11.1
mixture of hydroxides	$LaS(CeS)_{0.2}$-CrS_2	5	1.16	$LaS(CeS)_{0.2}$	6.0	6.0	11.3
				CrS_2	3.5	6.0	11.3
mixture of hydroxides	$LaS(GdS)_{0.2}$-CrS_2	3	1.17	$LaS(GdS)_{0.2}$	5.94	5.94	11.2
				CrS_2	3.48	5.94	11.2
mixture of hydroxides	$LaS(EuS)_{0.1}$-CrS_2	4	1.16	$LaS(EuS)_{0.1}$	5.86	5.86	11.3
				CrS_2	3.42	5.86	11.3
mixture of hydroxides	$CeS(GdS)_{0.2}$-CrS_2	5	1.16	$CeS(GdS)_{0.2}$	5.93	5.93	11.2
				CrS_2	3.47	5.93	11.2

[a] Lattice parameters of the same bulk misfit compound subunits are given in parentheses. Yields are given on a relative scale from 5 to 1, where 5 is the highest. See also the Supporting Information, Table S2.

transfer between the layers. The pseudo hexagonal layers of CrS_2 have three equivalent axes with 60° orientation angles (Supporting Information, Figure S2). As the LaS layers have a common *b*-axis with the CrS_2 layer (in the commensurate direction), they experience similar chemical environments in the three directions of the CrS_2 layers. This strong interaction between the layers also explains the observation of the same chiral angle for the CrS_2 and LaS layers.

Table 1 summarizes all of the LnS-TS_2 (T = Cr,V) nanotubular structures in the rare-earth-based family of misfit compounds that have been synthesized to date. SEM and TEM analyses of CeS-CrS_2 and GdS-CrS_2 nanotubes obtained during this study are given in the Supporting Information, Figures S3 and S4. The superstructure periodicity can be manipulated by alloying. For example, in 20 at% Gd-substituted $LaCrS_3$, new types of periodicities, such as O-T-O-T-T are observed (Supporting Information, Figure S5). Again, perfect periodicity of the layer superstructure is obtained, indicating strong charge interaction. The substitution of La by up to 20 at% with Ce, Eu, Gd, or Sr[15] atoms leds to the formation of quaternary nanotubular structures (see Table 1). Substitution of divalent ions, such as Sr^{2+} and Eu^{2+} (Eu forms a divalent ion in reducing conditions) at a concentration of more than 20 at% inhibits the MLC formation and leads to formation of nanowhiskers instead of nanotubes/nanoscrolls. The above observation explains the significance of misfit strain between LnS and TS_2 to scroll the structure.

Nanotubes of the misfit compound CeS-CrS_2 were further investigated by using aberration-corrected scanning TEM (STEM) and chromatic and spherical aberration-corrected TEM[16] (see Figure 3). High-annular angle dark-field (HAADF) STEM images revealed the perfect periodicity of a single repeating unit, consisting of a single layer of CrS_2 and a Ce-S doublet (representing one CeS molecular layer). The use of chromatic aberration correction allowed for spectroscopic energy-filtered imaging with atomic resolution.[17] Element-specific images were obtained by selecting only those electrons that had been scattered inelastically by Cr L_{23} and Ce N_{23} core-loss excitations (Figure 3b). Elemental maps extracted after background subtraction followed the structural modulation observed in the HAADF STEM images. The concentration modulation for Ce and Cr alternates, with maxima coinciding with the edge projection of the tubular shell where the projected mass density is highest (see insets in Figure 3b).

HRTEM images, taken under optimized negative phase contrast conditions, reveal atomic helices with bright atom contrast (Figure 3c). The atomic resolution detail shows the local stacking sequences of the misfit compound superstructure directly (Figure 3d). The predominant in-plane orientation relationship is ⟨010⟩ CrS_2 ‖ ⟨010⟩ CeS. Other in-plane stacking configurations with larger periodicities, such as ⟨010⟩ CrS_2 ‖ ⟨110⟩ CeS and ⟨010⟩ CrS_2 ‖ ⟨130⟩ CeS, were also found, giving rise to the in-plane rotation between O-T units mentioned above. All of these variants are shown in Figure 3d; the upper O-T sequence is ⟨010⟩ CrS_2 ‖ ⟨130⟩ CeS and the lower sequence is ⟨010⟩ CrS_2 ‖ ⟨010⟩ CeS. The ratio of the dimensions of the primitive subcells along the *a*-axis, *a*(CeS)/*a*(CrS_2), is close to 5/3. The misfit nanotube composition is therefore well in agreement with the compositional formula $(CeS)_{1.2}CrS_2$.

To shed light on the growth mechanism, a series of experiments was conducted at different temperatures (Supporting Information, Figure S6) and for different sulfurization times at 825 °C (Supporting Information, Figure S7). Nucleation of nanotube growth starts at 800 °C and the formation of nanotubes is seen at and above 825 °C. These results indicate

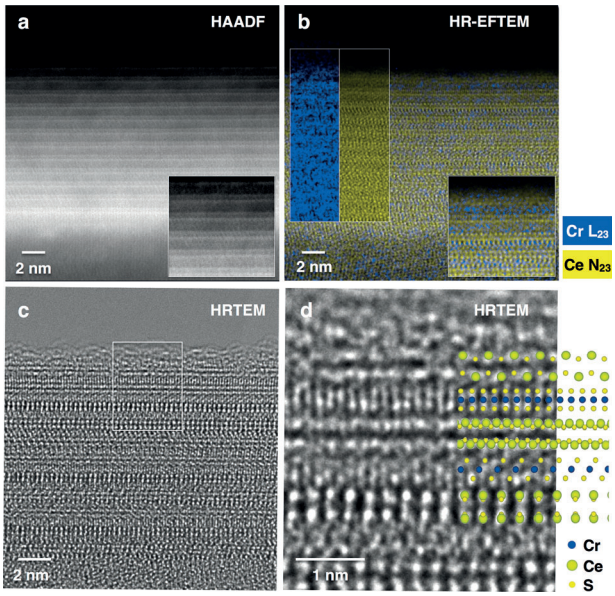

Figure 3. a) High-resolution HAADF STEM image of a CeS-CrS_2 nanotube. The high-angle scattering signal is highly sensitive to atomic number, with CeS double layers appearing bright against sandwiched CrS_2 layers. The inset shows a magnified region of the outer shells. b) Atomic-resolution energy-filtered TEM elemental maps taken using energy-selecting windows of 20 and 25 eV, corresponding to the Ce N_{23} and Cr L_{23} core-loss excitations, respectively. The modulation in the color-coded images obtained from the Ce and Cr signals shows the atomic-layer modulation. Inset: a magnified region of the outer shells. c) HRTEM images taken under optimized phase contrast conditions, with the projections of the atomic helices corresponding to bright dots. d) Magnified region of (c) with superimposed crystallographic projections of CeS double layers and hexagonal CrS_2 layers. The orientation relationship between the layers is described in the text.

that the growth mechanism of the La-based MLC is different from that of SnS-SnS_2 or PbS-NbS_2 nanotubes, which were obtained from nanoscrolls.[18] The following growth mechanism for Ln-based nanoscrolls/nanotubes is proposed. In the first heating step, the hydroxide mixture converts into porous $LaCrO_3$, which serves as a substrate for further nanotube growth. The reaction of $LaCrO_3$ with H_2S converts the oxide into a sulfide by a slow diffusion-controlled process. Strain is generated between the substrate and the freshly formed sulfide owing to the large difference in density between the precursor and the product (6.77 $g\,cm^{-3}$ for $LaCrO_3$; 4.66 $g\,cm^{-3}$ for $(LaS)_{1.2}CrS_2$), which results in large volumetric changes (one mole of the oxide occupies 35.3 cm^3, whereas that of the sulfide occupies 68.8 cm^3). Moreover, the thermal expansion coefficients of the sulfides are generally higher than those of the oxides, especially at higher temperatures, increasing strain during oxide to sulfide conversion. One stress relaxation process involves the growth of nanosheets of sulfide normal to the oxide substrate surface (especially from cracks). The growth of such stress-induced nanowhiskers or nanosheets has been reported.[18] The misfit stress between the LaS and CrS_2 sub-lattices further induces scrolling, corresponding to another stress-release process. The nanotubes/scrolls then continue to grow in length (root growth) and in diameter with increasing reaction time (Supporting Information, Figure S7). The density of the nanotubes depends on the number of grain boundaries available on the oxide substrate, which depends on reaction temperature and rate of heating. Thus, rapid heating of the precursor produces more nanotubes. Models of nanoscroll and nanotube growth are shown in the Supporting Information, Figures S8 and S9, respectively.

In conclusion, a new family of (lanthanide-based) misfit nanotubes/nanoscrolls was prepared. The synthesis procedure developed here, involving the high temperature transformation of the ternary oxide (hydroxide mixture) into the respective sulfide, provides a general method that can be used to synthesize a broad range of misfit nanotubes/nanoscrolls. The present study opens unique possibilities for further fundamental research in this field. By combining lanthanide ions with 3d transition metals or post-transition metals, one can make a wide variety of nanotubes from misfit chalcogenides with different properties. Optical characterization of LnS-TS_2 nanotubes reveals optical absorption in visible light range (Supporting Information, Figure S10), making them interesting for the study of light-induced effects in coupled layered electronic systems. Embedding the nanotubes in transparent matrices could lead to optically pumped emission lines with high quantum efficiency in the visible and IR range, which are suitable for many applications. Fascinatingly, any desired combination of insulators, semiconductors, metals, and superconductors with well-defined f–f optical transitions and magnetism can be made by the smart combination of elements. The resulting materials may find applications in fields that include thermoelectrics, light emitters, composites, magnetic materials, and catalysts and address fundamental physical issues in reduced dimensions.

Experimental Section

Synthesis of the precursors: Stoichiometric amounts (1:1) of $La(NO_3)_3{\cdot}6H_2O$ and $CrCl_3{\cdot}6H_2O$ were dissolved in milli Q water. While stirring, NH_4OH was added to the above solution to precipitate a mixture of $La(OH)_3$ and $Cr(OH)_3$. This hydroxide mixture was used as a precursor to produce LaS-CrS_2. Subsequent thermal annealing of the hydroxide mixtures ($La(OH)_3$ and $Cr(OH)_3$) at 900 °C in air yielded a $LaCrO_3$ powder.

Hydroxide mixtures of Ce, Gd, and Y with Cr were prepared in a similar manner to that described for La above, with $CeCl_3{\cdot}7H_2O$, $Gd(NO_3)_3{\cdot}6H_2O$, and $Y(NO_3)_3{\cdot}6H_2O$ used as sources of Ce, Gd, and Y, respectively.

Both precursors (a mixture of $La(OH)_3$ and $Cr(OH)_3$ or $LaCrO_3$) yielded nanotubes/nanoscrolls of LaS-CrS_2 when subjected to high temperatures in the presence of H_2/H_2S. In a typical reaction, the hydroxide mixture or oxide precursors were annealed at different temperatures in the presence of 40 sccm (standard cubic centimeters per minute) of 5 % H_2 + 95 % N_2 and 5 sccm of H_2S. Temperatures used were 650, 750, 825, 850, and 900 °C. Reactions with different annealing times at 825 °C were also conducted to understand the growth of the nanotubes.

Synthesis of nanotubes (nanoscrolls) of CeS-CrS_2 or GdS-CrS_2 and YS-CrS_2 was performed in a similar manner to that for LaS-CrS_2. Annealing a mixture of $Ce(OH)_3 + Cr(OH)_3$, a mixture of $Gd(OH)_3 + Cr(OH)_3$, or a mixture of $Y(OH)_3 + Cr(OH)_3$ in 40 sccm of 5 % H_2 + 95 % N_2 and 5 sccm of H_2S atmosphere at 850 or 900 °C yielded CeS-CrS_2, GdS-CrS_2, or YS-CrS_2 nanotubes, respectively. Nanotubes/nanoscrolls of LaS-VS_2 were synthesized by annealing

a mixture of $La(OH)_3 + VOSO_4 \cdot 5H_2O$ in 40 sccm of 5% H_2 + 95% N_2 and 5 sccm of H_2S atmosphere at 900 °C.

Quaternary nanotubular structures were prepared by substituting La by up to 20 at% with Ce, Eu, Gd, or Sr. The corresponding stoichiometric hydroxide mixtures were annealed at 850 °C in 40 sccm of 5% H_2 + 95% N_2 and 5 sccm of H_2S to obtain corresponding nanotubes.

SEM analysis was performed in a Zeiss Ultra V55 SEM. TEM analysis was performed in a Philips CM120 TEM operated at 120 kV, in an FEI Tecnai F20 TEM that was operated at 200 kV and equipped with STEM HAADF and in an FEI Tecnai F30-UT high-resolution TEM operated at 300 kV. Aberration-corrected TEM images and energy-filtered spectroscopic images were acquired in a chromatic and spherical aberration-corrected FEI Titan 60–300 Ultimate "PICO" instrument in the ER-C in Jülich. Probe-corrected STEM HAADF images were recorded using a semi-convergence angle of 30 mrad and an inner detector semi-angle of 89 mrad at an accelerating voltage of 200 kV. TEM images and EFTEM images were acquired at 200 kV using a chosen spherical aberration coefficient of −5 μm and a chromatic aberration coefficient of below 4 μm. Optimized phase contrast was achieved by acquiring images at a slightly positive defocus of + 5 nm, with a point resolution of better than 1 Å. EFTEM spectroscopic image series were recorded on a Gatan GIF Quantum ERS post-column imaging spectrometer using an energy step of 10 eV and a total of ten images per series. The axial chromatic aberration coefficient was below 4 μm, the chromatic astigmatism below 2 μm, and the chromatic dispersion coefficients below 50 nm. Energy-filtered images were taken at a defocus setting corresponding to minimum contrast in zero-loss filtered images. An energy-selecting slit width of 25 eV (20 eV) and an exposure time of 20 s (30 s) per series frame was used for recording the Cr L_{23} (Ce L_{23}) core loss at 575 eV (883 eV) energy loss. Elemental maps were calculated from spectroscopic image series following sub-pixel image alignment and pixel-wise background optimization and subtraction.

Received: April 10, 2014
Published online: June 4, 2014

Keywords: chalcogenides · lanthanides · misfit-layered compounds · nanotubes

[1] S. Iijima, *Nature* **1991**, *354*, 56 – 58.
[2] a) R. Tenne, L. Margulis, M. Genut, G. Hodes, *Nature* **1992**, *360*, 444 – 446; b) L. Margulis, G. Salitra, R. Tenne, M. Talianker, *Nature* **1993**, *365*, 113 – 114; c) Y. Feldman, E. Wasserman, D. J. Srolovitz, R. Tenne, *Science* **1995**, *267*, 222 – 225; d) R. Tenne, *Nat. Nanotechnol.* **2006**, *1*, 103 – 111.
[3] G. Seifert, T. Kohller, R. Tenne, *J. Phys. Chem. B* **2002**, *106*, 2497 – 2501.
[4] C. N. R. Rao, A. Govindaraj, *Nanotubes and Nanowires*, RSC Publishing, Cambridge, UK, **2005**.
[5] a) G. A. Wiegers, *Prog. Solid State Chem.* **1996**, *24*, 1 – 139; b) E. Makovicky, B. G. Hyde in *Structure and Bonding*, *Vol. 46*, Springer, Heidelberg, **1981**, p. 101; c) G. A. Wiegers, A. Meerschaut in *Materials Science Forum*, *Vol. 100 & 102* (Ed.: A. Meerschaut), Trans. Tech Publications, Switzerland, **1992**, p. 101; d) M. Kars, D. C. Fredrickson, A. Gómez-Herrero, S. Lidin, A. Rebbah, L. C. Otero-Diáz, *Mater. Res. Bull.* **2010**, *45*, 982 – 988.
[6] a) G. A. Slack in *CRC Handbook of Thermoelectric* (Ed.: D. M. Rowe), CRC Press, Boca Raton FL, **1995**, pp. 407 – 440; b) E. Putri, C. Wan, Y. Wang, W. Norimatsu, M. Kusunoki, K. Koumoto, *Scr. Mater.* **2012**, *66*, 895 – 898.
[7] a) D. Reefman, J. Baak, H. B. Brom, G. A. Wiegers, *Solid State Commun.* **1990**, *75*, 47 – 51; b) L. Schmidt, S. L. McCarthy, J. P. Maita, *Solid State Commun.* **1970**, *8*, 1513 – 1515; c) L. Schmidt, *Phys. Lett. A* **1970**, *31*, 551 – 552.
[8] a) D. Bernaerts, S. Amelinckx, G. Van Tendeloo, J. Van Landuyt, *J. Cryst. Growth* **1997**, *172*, 433 – 439; b) S. Y. Hong, R. Popovitz-Biro, Y. Prior, R. Tenne, *J. Am. Chem. Soc.* **2003**, *125*, 10470 – 10474.
[9] G. Radovsky, R. Popovitz-Biro, D. G. Stroppa, L. Houben, R. Tenne, *Acc. Chem. Res.* **2014**, *47*, 406 – 416.
[10] K. Kato, I. Kawada, T. Takahashi, *Acta Crystallogr. Sect. B* **1977**, *33*, 3437 – 3443.
[11] F. M. R. Engelsman, G. A. Wiegers, F. Jellinek, B. Van Laar, *J. Solid State Chem.* **1973**, *6*, 574 – 582.
[12] G. A. Wiegers, *J. Alloys Compd.* **1995**, *219*, 152 – 156.
[13] L. Yi, M. Zheng, Z. Yan-Fei, M. Singh, W. Jian, *Chin. Phys. B* **2013**, *22*, 067302.
[14] J. E. Mooij, Y. V. Nazarov, *Nat. Phys.* **2006**, *2*, 169 – 172.
[15] L. Cario, D. Johrendt, A. Lafond, C. Felser, A. Meerschaut, J. Rouxel, *Phys. Rev. B* **1997**, *55*, 9409 – 9414.
[16] M. Haider, P. Hartel, H. Müller, S. Uhlemann, J. Zach, *Microsc. Microanal.* **2010**, *16*, 393 – 408.
[17] a) K. W. Urban, J. Mayer, J. R. Jinschek, M. J. Neish, N. R. Lugg, L. J. Allen, *Phys. Rev. Lett.* **2013**, *110*, 185507; b) B. Kabius, P. Hartel, M. Haider, H. Müller, S. Uhlemann, U. Loebau, J. Zach, H. Rose, *J. Electron Microsc.* **2009**, *58*, 147 – 155.
[18] a) R. Takagi, *J. Phys. Soc. Jpn.* **1957**, *12*, 1212 – 1218; b) A. M. B. Gonçalves, L. C. Campos, A. S. Ferlauto, R. G. Lacerda, *J. Appl. Phys.* **2009**, *106*, 034303.

